(This is a sample cover image for this issue. The actual cover is not yet available at this time.)

Earth and Planetary Science Letters 312 (2011) 237–242

Contents lists available at SciVerse ScienceDirect

Earth and Planetary Science Letters

journal homepage: www.elsevier.com/locate/epsl

Crystal structure prediction for iron as inner core material in heavy terrestrial planets

Stefaan Cottenier [a,b,*], Matt I.J. Probert [c], Tim Van Hoolst [d], Veronique Van Speybroeck [a], Michel Waroquier [a]

[a] Center for Molecular Modeling & QCMM Alliance Ghent-Brussels, Ghent University, Technologiepark 903, BE-9052 Zwijnaarde, Belgium
[b] Department of Materials Science and Engineering, Ghent University, Technologiepark 903, BE-9052 Zwijnaarde, Belgium
[c] Department of Physics, University of York, Heslington, York, UK
[d] Reference Systems and Planetology, Royal Observatory of Belgium, Ringlaan 3, BE-1180 Brussels, Belgium

ARTICLE INFO

Article history:
Received 23 July 2011
Received in revised form 16 September 2011
Accepted 26 September 2011
Available online xxxx

Editor: T. Spohn

Keywords:
inner core
terrestrial exoplanets
iron
crystal structure prediction
quantum mechanics
density functional theory

ABSTRACT

The relative stability of different crystal structures for pure Fe under applied pressure is calculated from quantum mechanics, using the highly accurate APW + lo method. In the pressure range of 0–100 TPa, we corroborate the prediction that iron adopts subsequently the bcc, hcp, fcc, hcp and bcc structures. In contrast to previous studies, we identify a family of stacking fault structures that are competing with the ground state structure at all pressures. Implications for the properties of the inner core of the Earth and heavy terrestrial exoplanets are discussed.

1. Introduction

It has become a routine practice nowadays in computational condensed matter physics to predict properties of a given solid based on nothing more than the fundamental laws of quantum physics (Hafner, 2008; Hafner et al., 2006; Segall et al., 2002; Wentzcovitch and Stixrude, 2010). The only input that is required, is an (approximate) description of the crystal unit cell: space group, lattice parameters, unit cell angles and Wyckoff positions. The predictive capabilities of these so-called '*ab initio*' or '*first-principles*' calculations are currently being pushed one step further, by dropping the requirement of supplying the crystal unit cell as input. It has become feasible to take as input only the chemical composition of a material (i.e. the type and number of elements in the unit cell), and leave the task of determining the lowest energy crystal structure to quantum physics (Woodley and Catlow, 2008). This approach is particularly useful in situations where it is difficult to obtain experimental information on the crystal structure, e.g. when the material is subject to extreme pressures and or temperatures.

The emerging possibility of *ab initio* crystal structure prediction requires efficient methods to search through the infinite space of possible crystal structures, and doing so within a finite time span. A considerable set of algorithms is now available for this purpose (Woodley and Catlow, 2008), of which we list here three that are used in particular for solids: the *random search method* (Freeman and Catlow, 1992; Pickard and Needs, 2006, 2009a,b, 2010a,b), a *genetic algorithm* (Abraham and Probert, 2006; Abraham and Probert, 2008; Glass et al., 2006; Oganov et al., 2006; Oganov and Glass, 2006; Oganov et al., 2007; Oganov et al., 2009) and *database mining* (Curtarolo et al., 2003; Curtarolo et al., 2005; Fischer et al., 2006). The random search method is conceptually most simple: a series of random unit cells with the specified chemical composition is generated, and each cell is geometry-optimized using tools that are available in nearly any *ab initio* code. This procedure maps every random guess to a local minimum in the search space, and the hope is that after a moderate amount of trials the global minimum will be among them. A genetic algorithm starts from a set of random guesses too, but this set is much smaller. After geometry-optimization to the nearest local minimum, the lowest-energy structures of the set are combined into a new structure, that is hoped to 'inherit' good properties from both 'parents'. This survival of the fittest goes on for a few generations, until the absence of further improvement indicates that the global minimum has (probably) been found. *Ab initio* data mining has a very different strategy. A database is created for a given type of formula unit (e.g. A_2B_3, where A and B run across the periodic table). For every chemical formula within this set, the total energy is computed for a (large) set of crystal structures that are compatible with this formula unit. A statistical analysis

* Corresponding author.
E-mail address: Stefaan.Cottenier@ugent.be (S. Cottenier).

0012-821X/$ – see front matter © 2011 Elsevier B.V. All rights reserved.
doi:10.1016/j.epsl.2011.09.045

subsequently points out correlations between crystal structures and energies in the set. By these correlations, predictions are possible for *all* structure types in the set based on *ab initio* calculations for only a few of them. This tremendously reduces the time needed to predict the structure for a new compound. A disadvantage of this method is that it cannot predict any new structure type that was not included in the initial set, and that it requires quite some work to build the initial data base. A random search and a genetic algorithm do not suffer from these problems, but their disadvantage is that every new prediction takes as much time as the previous one — there is no learning process as for data mining.

These new structure prediction tools have been applied in the recent past to problems that are of interest to Earth and planetary science (Oganov et al., 2006; Pickard and Needs, 2009b). The motivation is the lack of experimental structure information for solids subject to the high pressures and/or high temperatures in planetary interiors, which often cannot be reproduced in lab conditions. An example of such a problem is the deceivingly simple question of the crystal structure of the inner core material of terrestrial planets (Dubrovinsky et al., 2007; Ekholm et al., 2011; Mikhaylushkin et al., 2007; Oganov et al., 2005; Steinle-Neumann et al., 2001; Stixrude and Cohen, 1995; Tateno et al., 2010; Vočadlo et al., 2003; Vočadlo, 2007). In a first approximation, the chemical composition of such inner cores can be taken to be pure iron. In the Earth, this material is subject to a pressure of about 350 GPa and a temperature of 6000 K. A genetic algorithm search by Oganov et al. has shown (Oganov et al., 2005) that at 0 K and 350 GPa, pure iron adopts the hexagonal close packed (hcp) structure (there is a well-known phase transition from the bcc-Fe phase at ambient conditions to hcp-Fe at 14 GPa (Dewaele et al., 2006; Mao et al., 1990; Takahashi and Basset, 1964). In other planets, the pressure can be considerably higher. For example, the central pressure in Jupiter, which may contain an ice–rock–iron core, is about 4 TPa (Guillot and Gautier, 2007). More massive exoplanets exist with consequently larger central pressures (Schneider et al., 2011). Even exoplanets with an Earth-like composition and presumably an iron core beneath a silicate shell have been detected, with core pressures in the TPa range. A lower limit to the pressure in their core can be calculated as $P_c = 3GM^2/(8\pi R^4)$ by assuming the density to be homogeneous. This underestimates the central pressure by a factor two for the Earth and even more for more massive planets. The planet CoRoT-7b, probably the first known super-Earth (Queloz et al., 2009), has an estimated mass of 5.2 ± 0.8 M_{Earth} and a radius of 1.58 ± 0.10 R_{Earth} (Bruntt et al., 2010), indicating a central pressure of a few times 0.74 TPa. Theoretical models of the interior structure of terrestrial type exoplanets show that pressures in the iron core can be up to almost 10 TPa for masses of about 10 M_{Earth} and up to 50 TPa for masses of 100 M_{Earth} (Grasset et al., 2009; Seager et al., 2007; Valencia et al., 2007).

Studying inner core material in this unexplored TPa range was one of the motivations for a recent work by Pickard & Needs (Pickard and Needs, 2009b), where the random search method was used to predict the crystal structure of pure Fe up to 50 TPa (at 0 K). They examined unit cells with 4, 6, 8 and 10 atoms, and concluded that no other structures than the high-symmetry bcc, fcc and hcp structures were competing for the ground state. The hcp phase remains the most stable one up to 8 TPa, a pressure at which the fcc phase takes over. At 24 TPa, hcp has the lowest energy again, and at 35 TPa there is a dramatic take-over by the bcc-phase (dashed lines in Fig. 1).

The bcc–hcp–fcc–hcp–bcc pressure sequence for pure iron is an interesting result, which triggers new questions. Before anything else, one can wonder about the reliability of this result. Total energies in the random search by Pickard & Needs have been obtained by density functional theory, using a plane wave basis set and pseudopotentials. A pseudopotential replaces the atomic-like region near the nucleus, where the wave functions vary steeply, with a much 'softer' potential that removes the sharp peaks from the wave functions. A good pseudopotential should affect only the core region of the atom, and should not disturb the behavior in the valence region, which is where the chemistry happens. Pseudopotentials are unavoidable if one wants to use a plane wave basis set, as the number of basis functions needed to describe the steep but otherwise uninteresting parts of the wave functions close to the nuclei would be prohibitively large. Nevertheless, the introduction of a pseudopotential is always a potentially dangerous action, that might lead to artifacts and unphysical results. Plane wave calculations for a given pseudopotential must be checked with respect to results obtained by so-called 'all-electron' calculations, which use a more complex type of basis functions and which therefore allow to work with the unmodified, true potential. This has been done extensively in the past for Fe pseudopotentials that are used for plane wave calculations for common Fe-containing solids. The extremely short Fe–Fe-distances in Fe under GPa and TPa pressures, however, forced Pickard & Needs to generate a new, dedicated pseudopotential: the pseudized regions of two neighboring atoms should not overlap, and with common Fe pseudopotentials at these pressures this does happen. Therefore, before accepting the predicted high-pressure behavior of Fe as numerically correct, a thorough verification with an all-electron method is required. A second question, of quite a different nature, deals with the absolute reliability of the predicted high-pressure phases. Only unit cells with 4, 6, 8 and 10 atoms were examined by Pickard & Needs. While this is good as a first survey, it certainly doesn't cover all possibilities. In order to find out whether relevant phases might have been missed, more work is needed.

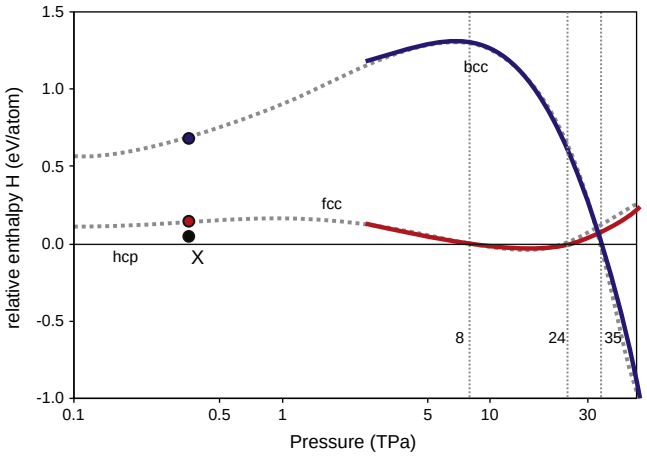

Fig. 1. Comparison of the 0 K relative enthalpy for fcc-Fe and bcc-Fe with respect to hcp-Fe, as a function of pressure (logarithmic scale). Smooth dotted lines are the pseudopotential results by Pickard and Needs, 2009b. Full lines as well as the 0.35 TPa values for bcc and fcc are all-electron results from this work. Vertical dotted lines indicate the transition pressures between the different phases. The 0.35 TPa value for structure X is a pseudopotential result obtained in this work.

The present paper has two goals. First, we will examine the pressure sequence of the high-symmetry phases of Fe with an all-electron method, in order to assess the reliability of the high-pressure pseudopotentials used by Pickard & Needs. Secondly, we will do a rather basic structure prediction attempt for Fe with only 3 atoms in the unit cell — simpler than all cases studied by Pickard & Needs. This will yield a structure that does compete with the high-symmetry phases, and that has given us the inspiration to examine the behavior of a family of stacking-fault based crystal structures under pressure. This will eventually lead us to the conclusion that the crystal structure of the inner cores of the Earth and heavy terrestrial planets might show a complex coexistence of many stacking faults.

2. Computational methods

All calculations in this work were done within the framework of Density Functional Theory (Cottenier, 2002; Hohenberg and Kohn, 1964; Kohn and Sham, 1965), using the Perdew–Burke–Ernzerhof exchange-correlation functional (Perdew et al., 1996). Two different numerical methods were used for solving the scalar-relativistic Kohn–Sham equations for periodic solids. The first one is the plane wave plus pseudopotential method as implemented in the CASTEP code (Segall et al., 2002). This method was applied at relatively low pressures only, using a standard ultrasoft pseudopotential for Fe. A basis set size determined by a plane wave energy cut-off of 600 eV was taken, and a mesh of $14\times14\times9$ k-points was used to sample the Brillouin zone. The second method is the all-electron Augmented Plane Waves + local orbitals (APW + lo) method (Cottenier, 2002; Madsen et al., 2001; Sjöstedt et al., 2000) as implemented in the WIEN2k package (Blaha et al., 1999). In this method the wave functions are expanded into spherical harmonics inside nonoverlapping atomic spheres of radius R_{MT} and in plane waves in the remaining space of the unit cell (= the interstitial region). As we applied this method for calculations at very high pressures and correspondingly small interatomic distances, we took an extremely small value of $R_{MT}^{Fe}=0.97$ a.u. This is mandatory in order to avoid overlapping spheres. The charge density was Fourier expanded up to $G_{\max}=20\sqrt{Ry}$. The plane wave expansion of the wave function in the interstitial region was truncated at a very large value of $K_{\max}=7.0/R_{\mathrm{MT}}^{\min}=7.22$ a.u.$^{-1}$, which leads to very accurate values for the calculated energies. A very dense mesh of k-points was taken, corresponding to a $30\times30\times30$ mesh for a conventional fcc unit cell at ambient pressure. The mesh for the fast Fourier transform that is needed to calculate the exchange-correlation potential in the interstitial region, was taken 6 times denser than usually done, due to the very small sphere sizes. The procedure to choose the linearization energies is discussed in Section 3.1 and Appendix A.

3. Results and discussion

3.1. Assessment of the pseudopotential quality

Although all-electron methods as APW + lo do not suffer from the need to generate a good-quality pseudopotential first, their application to solids as exotic as iron at a few TPa of pressure is not straightforward either. A key feature in the APW + lo method is to select appropriate values for the so-called 'linearization energies' (Andersen, 1975; Singh, 1994). Based on extensive experience for conventional solids, robust algorithms are available to provide suitable linearization energies in an automated way. For the present non-standard application, however, a manual tuning is required. We calculated the Density of States (DOS) for hcp, fcc and bcc Fe at 20 different volumes that covered the entire range of interest. From these DOS plots, appropriate linearization energies were selected. Those were subsequently fit with polynomial functions, such that a linearization energy at any volume in the interval could be generated. A plot of the linearization energies can be found in Fig. A.5. Another complication is that for the APW + lo basis no stress tensor formalism has been developed yet. As a result, calculations cannot be performed at a given pressure, but only at a given volume. The pressure can only be determined *a posteriori*, as the opposite of the numerically obtained first derivative of the energy–versus–volume curve. In order to do that in a numerically stable way, energies at a lot of volumes should be available. We used a volume difference of 0.08 Å^3 between two subsequent calculations in the 'low pressure' range ($\leq$10 TPa), and decreased this in several steps up to 0.02 Å^3 for the highest pressures.

The result of APW + lo calculations for bcc, hcp and fcc Fe are shown in Fig. 1, and compared with the plane wave calculations by Pickard & Needs. The agreement is excellent. This confirms that the high-pressure Fe pseudopotential developed by Pickard & Needs does not introduce unphysical artifacts.

3.2. Random search with 3 atoms per cell

Pickard & Needs examined only cases with an even number of Fe atoms per unit cell, from 4 to 10 atoms per cell. The reason for this choice is clear: a cell with e.g. 3 atoms per cell can also be described by its doubled unit cell, which contains 6 atoms. Simulations with 4, 6, 8 and 10 atoms per cell therefore effectively cover all possible cases from 1 to 10 atoms per cell, except for 7 and 9 atoms. However, as there are many more combinations possible with 2×3 atoms than with 3 atoms, a search with 3 atoms should find the global minimum with less random trials than a search with 6 atoms. This motivated us to perform a modest random search for cases with only 3 Fe atoms in the unit cell, using the same CASTEP plane wave code that was used by Pickard & Needs. We performed this search at an applied pressure of 350 GPa only, where the Fe–Fe distances are still large enough to allow to use a regular Fe pseudopotential. From this search, a structure emerged with an enthalpy that is at 350 GPa only 0.05 eV/atom above the enthalpy of the hcp phase, and 0.08 eV/atom *below* the enthalpy of the competing fcc phase (Fig. 1). We will denote it further as structure 'X'. The full crystal structure information of structure X, obtained by APW + lo at 3 typical pressures, is given in Table 1.

Closer examination of this structure shows that it is intimately related to the hcp and fcc structures. The hcp structure can be described as an infinitely alternating A–B stacking of close-packed {001} layers (see Fig. 2): …*ABABABAB*…. Modifications to this perfect hcp sequence represent defects in the material. Three well-known defects are classified as *stacking faults*, and are labeled in the terminology of Hirth and Lothe (Hirth and Lothe, 1982) by I_1, I_2 and E. They have the following structure: …*ABABACAC*… (I_1, remove one B-layer from the original hcp sequence, and shift all layers at the right of it by $\vec{t_C}$), …*ABABCACA*… (I_2, shift all layers at the right of a given layer by $\vec{t_C}$) and …*ABABACBABAB*… (E, insert a C layer into the hcp sequence). Other possible defects that are no stacking faults are T_2 (…*ABABCBABA*…: mirror symmetry about the faulted C-layer) and the 6H structure …*ABACAB*… (Inoue et al., 2002). The fcc structure is a A–B–C alternation of {001} planes: …*ABCABCABC*…. The fcc structure can be considered as a damaged hcp structure, where after every 2 layers a I_2 stacking fault appears. The newly found competing structure X can be described with 9 layers per (non-primitive) unit cell: ABCBCACAB. It can be obtained by starting from hcp, and inserting a I_1 stacking fault at every third layer.

3.3. Stacking faults in a 6-layer system

Structure X contains 3 atoms per primitive unit cell, but can be described by a non-primitive cell with 6 atoms as well. In spite of this, it has not shown up as a result of the random search by Pickard & Needs, who did consider the case with 6 atoms per cell. This makes us wonder: are there other interesting crystal structures that might have been missed by this search? As we know now that stacking fault structures are promising candidates, we will systematically examine all different stacking sequences that have a repetition period of 6 layers. As every {001} layer can be described by a single atom, these are effectively unit cells with 6 atoms. There are only 4 inequivalent stacking sequences of this type: ABABAB (hcp), ABABAC (one I_1 fault per 6 layers, referred to as α hereafter), ABACBC (one I_2 fault per 6 layers, referred to as β hereafter) and ABCABC (fcc, three I_2 faults per 6 layers). Any other stacking sequence with a periodicity of 6 layers can be reduced to one of these four by symmetry. The fact that the high-symmetry structures hcp and fcc are both part of this set, makes the 6-layer system a very suitable model system to examine.

Table 1
Crystallographic information of pure iron in space group C/2m (space group nr. 12, unique axis c), as calculated with the APW + lo method at 4 relevant pressures P (TPa): lattice parameters a, b and c (Å), cell angle γ°, free parameters x and y in the 4i Wyckoff position, primitive cell volume V (Å^3), smallest Fe—Fe distance d (Å) and density (kg/m^3).

P	a	b	c	γ	x	y	V	d	
0	4.2559	6.5199	2.4571	115.7868	0.5584272	0.3376933	30.695	2.375	9,063.2
0.35	3.6622	5.6379	2.1144	115.6991	0.5569537	0.3355993	19.669	2.069	14,144
5	2.7818	4.3336	1.6061	115.0806	0.5552566	0.3329378	8.768	1.601	31,729
50	2.0853	3.2853	1.2040	115.0911	0.5553703	0.3330570	3.375	1.204	82,429

The results are shown in Fig. 3. At low pressures, the two 6-atom stacking fault structures both have an enthalpy that is higher than hcp, but *lower* than fcc. The enthalpy of the 3-atom stacking fault structure X described in the previous section, is of a comparable magnitude. This means that all of these structures are competing for the ground state — there is nothing particularly special about structure X, many stacking fault structures will exist that have enthalpies between hcp and fcc. And none of these had spontaneously emerged from the random search by Pickard & Needs. At about 8 TPa, there is a qualitative change: the low-pressure enthalpy order α<X<β<fcc is almost entirely reversed and becomes fcc<β <X =α. As already observed in Fig. 1, the enthalpy of the fcc phase drops below the enthalpy of hcp. None of the stacking fault structures, however, has at any pressure an enthalpy that is the absolute minimum. Between 30 and 50 TPa, the reversal is gradually undone, and the same sequence as appears at low pressures is restored. At those pressures, however, bcc has already taken over as the lowest-enthalpy structure.

3.4. Stacking faults in an N-layer system ($N \leq 10$)

Fig. 4 shows the enthalpy per atom (relative to hcp) for an exhaustive list of 46 stacking sequences with up to 10 layers per unit cell, calculated at 350 GPa with pseudopotentials and plane waves. The larger the number of layers, the more possibilities. The minimal enthalpy in this set is for hcp, of which the enthalpy is arbitrarily taken to be 0 eV/atom (hcp can be formed for N = 2, 4, 6, 8, 10). No stacking sequence drops below this value. The maximal enthalpy in the set turns out to be for fcc, which can be formed for N = 3, 6 and 9. The larger N, the smaller the enthalpy gap between hcp and the lowest-enthalpy stacking sequence. This does not suggest, however, that for even larger values of N these kinds of stacking sequences might drop below the hcp value. It is rather a consequence of plotting these data as eV per atom. It requires a given amount of energy to introduce one single stacking fault (e.g. I_1) into a perfect hcp lattice. When divided by the infinite number of atoms in the unit cell for such a case, the enthalpy difference per atom must go to zero. The low-lying data points in Fig. 4 are structures with one single defect per unit cell. The more atoms in the cell, the smaller the enthalpy difference per atom. As an example, cases with a single I_1 defect are marked by a square in Fig. 4 — they have indeed enthalpies that are among the lowest ones next to hcp.

Is it likely that any of the structures in Fig. 4 (which is made for 0.35 TPa) would drop below the enthalpy of the fcc structure at, say,

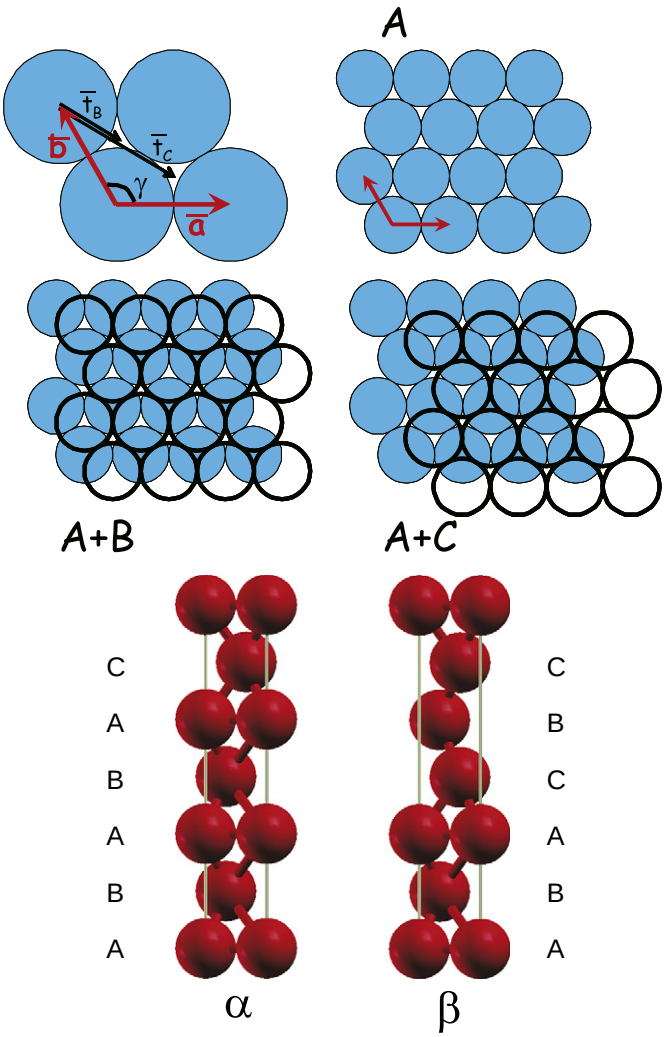

Fig. 2. Top view of a {001} plane in the hcp structure. Upper left: the lattice vectors $\vec{a}$ and $\vec{b}$, making an angle γ = 120° with each other. The vectors $\vec{t_B} = \frac{1}{3}\left(\vec{a} - \vec{b}\right)$ and $\vec{t_C} = \frac{2}{3}\left(\vec{a} - \vec{b}\right)$ are indicated as well. Upper right: a {001} layer is chosen as 'A'. Middle left: a B-layer is obtained by shifting the A-layer over $\vec{t_B}$. Middle right: a C-layer is obtained by shifting the A-layer over $\vec{t_C}$. Lower panel: side view of the unit cells of the α— and β-structures (N = 6) as defined in Table A.2 and used in Figs. 3 and 4.

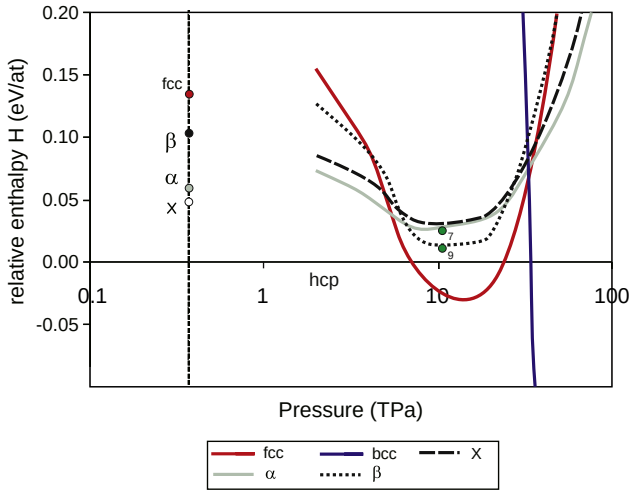

Fig. 3. Relative enthalpy of the bcc, fcc, α, β and X structures (see text) with respect to hcp, calculated by APW + lo as a function of pressure. The dashed vertical line indicates a typical Earth inner core pressure (0.35 TPa). The two single points at 11 TPa indicate the fcc-like structures with 7 and 9 atoms that are indicated as diamonds in Fig. 4.

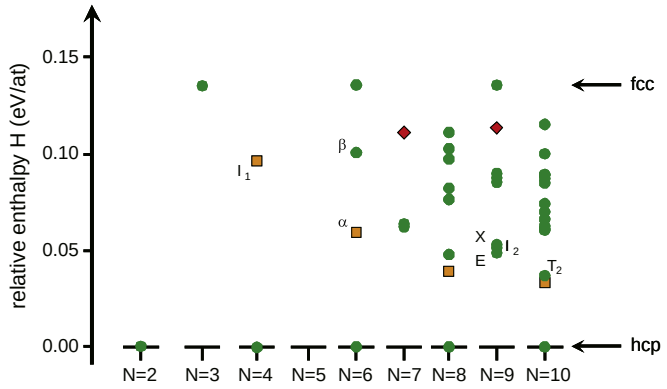

Fig. 4. Relative enthalpies (w.r.t. hcp) of all possible inequivalent stacking sequences for a given number of layers N, up to N = 10. Squares are structures with a single I_1 fault. The largest cell with a single I_2 fault, a single E fault, and a single T_2 fault, respectively, are labeled. The structures X (described with a non-primitive cell of 9 atoms) and α and β (N = 6) are labeled as well. Diamonds indicate the two fcc-like structures that are mentioned in Fig. 3.

11 TPa? It is tempting to have a closer look at some structures that have enthalpies as close as possible to the fcc value. We will do this for 2 cases, indicated by diamonds in Fig. 4: one with 7 atoms per unit cell (ABCABAC) and one with 9 atoms per unit cell (ABCABACBC), and at one pressure value (11 TPa). Cases with 7 and 9 atoms per unit cell were not covered in the study by Pickard & Needs. The results are given by the individual points in Fig. 3. Although they have enthalpies that are close to the hcp value, none of them drops below the fcc value. Given the systematics in Fig. 3, with a tendency to reverse the relative enthalpies at 11 TPa with respect to the situation at low pressure, it is unlikely that any of the other structures in Fig. 4 will become more favorable than fcc. This holds *a fortiori* for the structures with a single I_1, I_2, E or T_2 defect, which have at 0.35 TPa enthalpies that are closer to hcp than to fcc. Taken all together, this is a strong suggestion that for this pressure range and this class of structures, fcc has indeed the overall lowest enthalpy.

4. Conclusions and outlook

We assessed the quality of the high-pressure Fe pseudopotentials constructed by Pickard & Needs, by comparing their calculations for hcp, fcc and bcc Fe under pressure with all-electron calculations. The results are identical, which proves that this pseudopotential is reliable. We confirm that there is a pressure window (8–24 TPa) where the fcc structure is preferred over the hcp structure, and that beyond 37 TPa the bcc structure is the most stable one. We do not confirm, however, the conclusion by Pickard & Needs that only high-symmetry iron phases will compete for the ground state structure under high pressure. A modest random search has come up with a structure in space group C/2m that has an enthalpy that is never far away from hcp nor fcc. It can be interpreted as a stacking fault in the hcp structure. A systematic examination of periodic stacking fault sequences with a periodicity of up to 10 layers has shown that many similar structures exist that do compete for the ground state, albeit none of them has an enthalpy below the most stable simple phase (hcp, fcc or bcc) at any given pressure. Especially when considering the high temperatures present at the inner core of terrestrial planets (including the Earth), these results suggest that the crystal structure of the inner core material might be very complex, containing many stacking faults. It remains to be seen whether the presence of impurities in the inner core material might stabilize particular stacking faults, or even a radically different crystal structure.

These results may have implications for understanding the observed seismic anisotropy in the Earth. Seismic waves travel a few percent faster and are more attenuated for seismic paths parallel to the Earth's rotation axis than for paths parallel to the equator (Souriau, 2007). Moreover, the attenuation is depth-dependent and the uppermost 100–400 km is isotropic (e.g. Souriau, 2007), suggesting that the inner core may be layered (Sun and Song, 2008). Tentative explanations are based on the occurrence of different crystal structures, each with a high degree of alignment (e.g. (Ma et al., 2004)), and different orientations for every crystal structure. Our work suggests that varying densities of stacking faults are more likely to occur than varying crystal structures. If the stacking fault density would be correlated to the local orientation, this could lead to another way to understand the seismic anisotropy.

Acknowledgments

This work has been supported by the Fund for Scientific Research — Flanders (FWO) (Project. No. G.0402.11N), by the IWT-Vlaanderen through the ISIMADE project, and by the Research Board of Ghent University. S.C. acknowledges the financial support from OCAS NV by an OCAS-endowed industrial chair at Ghent University. Calculations were carried out using the Stevin Supercomputer Infrastructure at Ghent University, funded by the Ghent University, the Hercules Foundation and the Flemish Government — Department EWI.

Appendix A. Linearization energies

This Appendix elaborates on an important technical issue: the choice of linearization energies in the APW + lo method, for an exotic case as Fe under high pressure. The inset in Fig. A.5 shows the Fermi energy as a function of reduction of the volume relative to the equilibrium volume, for volumes that are 60% to 90% smaller than the equilibrium volume. The zero point on the Fermi energy scale is conventionally chosen such that it corresponds to the average value of the potential in the interstitial region. Fig. A.5 itself shows how the linearization energies are chosen with respect to this Fermi energy. The APW + lo basis set has functions with angular momentum ℓ ranging from 0 to 10. For $\ell = 4-10$, the linearization energy is taken 2.7 eV below the Fermi energy. For $\ell = 0-3$ (s, p, d, f), the linearization energy varies according to the "APW-spdf" line in Fig. A.5: 6 eV below the Fermi energy for the largest volumes, 50 eV below the Fermi energy for the smallest volumes. The local orbital basis functions in the basis set have linearization energies that vary according

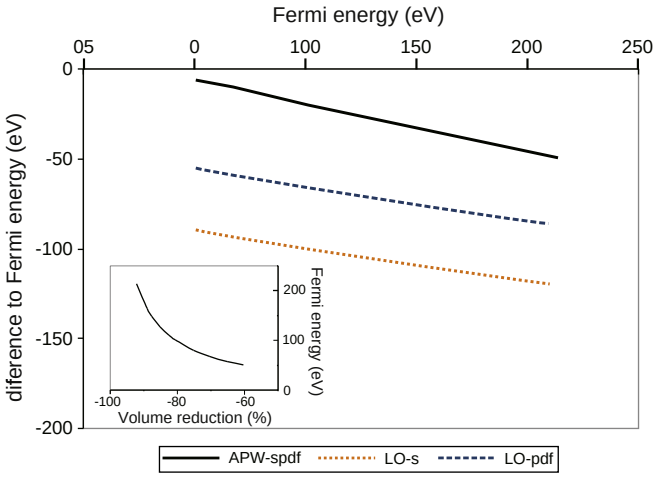

Fig. A.5. Linearization energies (eV) relative to the Fermi energy. Inset: Fermi energy (eV) relative to the volume reduction (%) w.r.t. the equilibrium volume.

Table A.2
For every value of the periodicity N ($2 \leq N \leq 10$), an exhaustive list of all inequivalent close-packed stackings is given, listed in order of decreasing enthalpy (highest enthalpy at the top of each column). The structures α, β and X from Fig. 3 are labeled. Stackings that are printed in bold can be described by a sequence with a smaller value of N as well.

N = 2	N = 3	N = 4	N = 5	N = 6	N = 7	N = 8	N = 9	N = 10
AB	ABC	ABAC	ABABC	**ABCABC**	ABACABC	ABACBABC	**ABCABCABC**	ABACABCABC
		ABAB		ABACBC$^{(\beta)}$	ABABABC	ABABCABC	ABACBACBC	ABACBACABC
				ABABAC$^{(\alpha)}$	ABABCAC	**ABACABAC**	ABABCABAC	ABACABACBC
				ABABAB		ABABCBAC	ABABCACBC	ABABCACBAC
						ABABACBC	ABABACABC	ABABACBABC
						ABABABAC	ABABCBCAC$^{(X)}$	**ABABCABABC**
						ABABACAC	ABABABCAC	ABABABCABC
						ABABABAB	ABABABABC	ABABCABCBC
								ABABCABCAC
								ABABACABAC
								ABABCBABAC
								ABABABCBAC
								ABABACACBC
								ABABABACBC
								ABABACBCBC
								ABABABABAC
								ABABABACAC
								ABABABABAB

to the "LO-s" line in Fig. A.5 if $\ell = 0$, and according to the "LO-pdf" line if $\ell = 1-3$.

Appendix B. Stacking sequences

This Appendix explains how the exhaustive list of stacking sequences for which the enthalpies are given in Fig. 4 has been obtained. Three types of layers (A, B and C) have to be stacked in a periodic way, with a period of N layers. This gives N^3 possibilities. Many of these N^3 stacking sequences are either irrelevant or equivalent, however. Four symmetry arguments allow to eliminate all redundant sequences. (1) As we are interested in close-packed stackings, no two subsequent layers should be identical (e.g.: for N = 7, ABBCBABA is not allowed). (2) The names A, B and C are a convention only. Permutations among them lead to equivalent stackings (e.g.: ABCBABC = BCACBCA = ACBCACB). (3) Due to periodic boundary conditions, the starting point of a sequence is arbitrary (e.g.: ABCBABA = BCBABAB). (4) There is no preferential up or down direction: inverting a sequence does not make a difference (e.g.: ABCBABA = ABABCBA). Applying these four symmetry operations to N = 10 ($10^3 = 1000$ possibilities) reduces the set to 18 inequivalent stackings. Table A.2 lists per value of N all inequivalent stackings, and this up to N = 10, according to decreasing enthalpy as in Fig. 4 (mind that for the largest values of N, several points in Fig. 4 are nearly overlapping).

References

Abraham, N.L., Probert, M.I.J., 2006. Phys. Rev. B 73, 224104.
Abraham, N.L., Probert, M.I.J., 2008. Phys. Rev. B 77, 134117.
Andersen, O.K., 1975. Phys. Rev. B 12, 3060.
Blaha, P., Schwarz, K., Madsen, G., Kvasnicka, D., Luitz, J., 1999. WIEN2k, An Augmented Plane Wave + Local Orbitals Program for Calculating Crystal Properties. Karlheinz Schwarz, Techn. Universität Wien, Austria3-9501031-1-2.
Bruntt, H., Deleuil, M., Fridlund, M., Alonso, R., Bouchy, F., Hatzes, A., Mayor, M., Moutou, C., Queloz, D., 2010. Improved stellar parameters of corot-7 a star hosting two super earths. Astron. Astrophys. 519, A51.
Cottenier, S., 2002. Density functional theory and the family of (L)APW-methods: a step-by-step introduction. Instituut voor Kern- en Stralingsfysica, KULeuven, Belgium90-807215-1-4. freely available from http://www.wien2k.at/reg_user/textbooks.
Curtarolo, S., Morgan, D., Persson, K., Rodgers, J., Ceder, G., 2003. Phys. Rev. Lett. 91, 135503.
Curtarolo, S., Morgan, D., Ceder, G., 2005. Calphad 29, 163.
Dewaele, A., Loubeyre, P., Occelli, F., Mezouar, M., Dorogokupets, P.I., Torrent, M., 2006. Phys. Rev. Lett. 97, 215504.
Dubrovinsky, L., Dubrovinskaia, N., Narygina, O., Kantor, I., Kuznetzov, A., Prakapenka, V.B., Vitos, L., Johansson, B., Mikhaylushkin, A.S., Simak, S.I., Abrikosov, I.A., 2007. Science 316, 1880.
Ekholm, M., Mikhaylushkin, A.S., Simak, S.I., Johansson, B., Abrikosov, I.A., 2011. Earth Planet. Sci. Lett. 308, 90.
Fischer, C.C., Tibbetts, K.J., Morgan, D., Ceder, G., 2006. Nat. Mater. 5, 641.
Freeman, C.M., Catlow, C.R.A., 1992. J. Chem. Soc. Chem. Commun. 2, 89.
Glass, C.W., Oganov, A.R., Hansen, N., 2006. Comput. Phys. Commun. 175, 713.
Grasset, O., Schneider, J., Sotin, C., 2009. Astrophys. J. 693, 722–733.
Guillot, T., Gautier, D., 2007. The Giant Planets. Volume 10 of Treatise on Geophysics. Elsevier.
Hafner, J., 2008. J. Comput. Chem. 29, 2044.
Hafner, J., Wolverton, C., Ceder, G., 2006. MRS Bull. 31, 659.
Hirth, J.P., Lothe, J., 1982. Theory of Dislocations. Wiley.
Hohenberg, P., Kohn, W., 1964. Phys. Rev. 136, B864.
Inoue, A., Matsushita, M., Kawamura, Y., Amiya, K., Hayashi, K., Koike, J., 2002. Mater. Trans. 43, 580.
Kohn, W., Sham, L.J., 1965. Phys. Rev. 140, A1133.
Ma, Y., Somayazulu, M., Shen, G., Mao, H., Shu, J., Hemley, R.J., 2004. Phys. Earth Planet. Inter. 143–144, 455–467.
Madsen, G.K.H., Blaha, P., Schwarz, K., Sjöstedt, E., Nordström, L., 2001. Phys. Rev. B 64, 195134.
Mao, H.K., Wu, Y., Chen, L.C., Shu, J.F., 1990. J. Geophys. Res. B 95, 21737.
Mikhaylushkin, A.S., Simak, S.I., Dubrovinsky, L., Dubrovinskaia, N., Johansson, B., Abrikosov, I.A., 2007. Phys. Rev. Lett. 99, 165505.
Oganov, A.R., Glass, C.W., 2006. J. Chem. Phys. 124, 244704.
Oganov, A.R., Price, G.D., Scandolo, S., 2005. Z. Krist. 220, 531.
Oganov, A.R., Glass, C.W., Ono, S., 2006. Earth Planet. Sci. Lett. 241, 95.
Oganov, A.R., Ma, Y., Glass, C.W., Valle, M., 2007. Ψ_k. Newsletter 84, 142.
Oganov, A.R., Chen, J., Gatti, C., Ma, Y.Z., Ma, Y.M., Glass, C.W., Yu, Z.L.T., Kurakevych, O.O., Solozhenko, V.L., 2009. Nature 457, 863.
Perdew, J.P., Burke, K., Ernzerhof, M., 1996. Generalized gradient approximation made simple. Phys. Rev. Lett. 77, 3865.
Pickard, C.J., Needs, R.J., 2006. Phys. Rev. Lett. 97, 045504.
Pickard, C.J., Needs, R.J., 2009a. Phys. Status Solidi B 246, 536.
Pickard, C.J., Needs, R.J., 2009b. J. Phys. Condens. Matter 21, 452205.
Pickard, C.J., Needs, R.J., 2010a. Nat. Mater. 9, 624.
Pickard, C.J., Needs, R.J., 2010b. Ψ_k. Newsletter 100, 42.
Queloz, D., Bouchy, F., Moutou, C., Hatzes, A., Hébrard, G., et al., 2009. Astron. Astrophys. 506, 303–319.
Schneider, J., Dedieu, C., Le Sidaner, P., Savalle, R., Zolotukhin, I., 2011. Defining and cataloging exoplanets: the exoplanet.eu database. Astron. Astrophys. 532. doi:10.1051/0004-6361/201116713.
Seager, S., Kuchner, M., Hier-Majumder, C.A., Militzer, B., 2007. Astrophys. J. 669, 1279.
Segall, M.D., Lindan, P.J.D., Probert, M.J., Pickard, C.J., Hasnip, P.J., Clark, S.J., Payne, M.C., 2002. J. Phys. Condens. Matter 14, 2717.
Singh, D., 1994. Planewaves, Pseudopotentials and the LAPW-method. Kluwer Academic Publishing.
Sjöstedt, E., Nordström, L., Singh, D.J., 2000. Solid State Commun. 114, 15.
Souriau, A., 2007. Treatise Geophys. 1, 655–693.
Steinle-Neumann, G., Stixrude, L., Cohen, R.E., Gülseren, O., 2001. Nature 413, 57.
Stixrude, L., Cohen, R.E., 1995. Geophys. Res. Lett. 22, 125.
Sun, X., Song, X., 2008. Earth Planet. Sci. Lett. 269, 56–65.
Takahashi, T., Basset, W.A., 1964. Science 145, 483.
Tateno, S., Hirose, K., Ohishi, Y., Tatsumi, Y., 2010. Science 330, 359.
Valencia, D., Sasselov, D.D., O'Connell, R.J., 2007. Astrophys. J. 656, 545.
Vočadlo, L., 2007. Treatise Geophys. 2, 91.
Vočadlo, L., Alfé, D., Gillan, M.J., Wood, I.G., Brodholt, J.P., Price, G.D., 2003. Nature 424, 536.
Wentzcovitch, R.M., Stixrude, L. (Eds.), 2010. Theoretical and Computational Methods in Mineral Physics: Geophysical Applications. : Volume 71 of Reviews in Mineralogy and Geochemistry. Mineralogical Society of America.
Woodley, S.M., Catlow, R., 2008. Nat. Mater. 7, 937.